

RSC Advances



This is an *Accepted Manuscript*, which has been through the Royal Society of Chemistry peer review process and has been accepted for publication.

Accepted Manuscripts are published online shortly after acceptance, before technical editing, formatting and proof reading. Using this free service, authors can make their results available to the community, in citable form, before we publish the edited article. This *Accepted Manuscript* will be replaced by the edited, formatted and paginated article as soon as this is available.

You can find more information about *Accepted Manuscripts* in the [Information for Authors](#).

Please note that technical editing may introduce minor changes to the text and/or graphics, which may alter content. The journal's standard [Terms & Conditions](#) and the [Ethical guidelines](#) still apply. In no event shall the Royal Society of Chemistry be held responsible for any errors or omissions in this *Accepted Manuscript* or any consequences arising from the use of any information it contains.

Necessity of moderate metal-support interaction in Ni/Al₂O₃ for syngas methanation at high temperatures

Dianmiao Cui^{a,b}, Jiao Liu^{a,*}, Jian Yu^a, Junrong Yue^a, Fabing Su^a, Guangwen Xu^{a,*}

^a State Key Laboratory of Multi-phase Complex Systems, Institute of Process Engineering, Chinese Academy of Sciences, Beijing 100190, China

E-mail: liujiao@ipe.ac.cn; gwxu@ipe.ac.cn; Fax: 86-10-82544886; Tel: 86-10-82544429

^b University of Chinese Academy of Sciences, Beijing 100049, China

Abstract: This article investigated the necessary metal-support interaction in Ni-Mg-Zr-La/Al₂O₃ catalyst for high-temperature syngas methanation through varying the calcination and reduction temperatures during catalyst preparation. Atmospheric syngas methanation was conducted continuously but at 823 K and 923 K alternatively. Raising the calcination temperature increased the interaction between nickel and alumina support but lowered the surface area of the catalyst. The catalyst calcined at the higher temperature such as 1073 K exhibited the highest initial activity in spite of its least active sites. However, only those catalysts with moderate interaction, such as that calcined at 973 K, showed stable activity of methanation above 823 K. Too small surface area of the catalyst calcined at too high temperatures, such as 1073 K, would lead to serious aggregation of nickel particles and thus cause carbon deposition during methanation. Varying the reduction temperature for the catalyst demonstrated that the excessive reduction of the nickel species such as reduced at 1073 K almost removed all the nickel aluminates to cause the catalyst to have low activity, quick nickel aggregation and carbon deposition. This further justified that moderate metal-support interaction is necessary to ensure the high

activity and stability of the Ni/Al₂O₃ catalyst for syngas methanation at high temperatures.

Keywords: Methanation, SNG, Ni/Al₂O₃, Interaction, Calcination, Reduction

1. Introduction

Production of synthetic natural gas (SNG) via methanation of syngas, which can be derived from coal or renewable biomass, has received widespread attention due to the lacking of natural gas in China. The methanation of carbon monoxide ($\text{CO} + 3\text{H}_2 \rightarrow \text{CH}_4 + \text{H}_2\text{O}$, $\Delta H = -206.28 \text{ KJ} \cdot \text{mol}^{-1}$) is highly exothermic and thus requires the catalyst to possess high activity at low temperature (ca. 523 K) and high stability at high temperature (ca. 923 K). Ni-based catalysts have been widely used for syngas methanation due to its relatively high intrinsic activity and low price. The activity of Ni-based catalyst depends on numbers of factors including the composition or crystal size of active metal,¹⁻⁴ nature properties of active metal and support⁵⁻⁸ and physio-chemical interaction between active sites and support.⁹⁻¹² The activity of the catalyst would decrease with carbon deposition,¹³ sintering of active metal and/or support,¹⁴⁻¹⁷ Ni loss and poisoning^{18, 19} and so on. Numerous studies of Ni catalysts for CO disproportionation, methane reforming and decomposition of hydrocarbons have shown that the deactivation of catalysts was usually initiated with formation of filamentary carbon that has graphite-like structure.²⁰⁻²³ In order to improve the stability and carbon resistance, alkali and alkaline earth metal oxides as well as rare earth oxides were usually added to modify the nickel catalyst.^{24, 25}

On the other hand, catalytic performance of the nickel-based catalysts strongly

depends not only on the nature and structure of active nickel but also on the chemical and physical property of supporting materials. Various materials, such as Al_2O_3 , TiO_2 , SiO_2 and SiC , have been investigated as support for Ni catalysts,^{14, 26-28} but Al_2O_3 is still the most widely applied.^{29, 30} The Al_2O_3 support could weaken the interaction among Ni particles to stabilize the NiO particles against sintering. At high calcination temperatures, nickel oxide and nickel aluminates are formed. Nickel aluminates render the reduction of the nickel oxide more difficult and lead to a decrease in the number of active sites and thus catalytic activity of the catalyst. Meanwhile, a relatively strong interaction between the nickel species and alumina support could result in finely dispersed nickel particles on the catalyst surface and thereby prevent the coke formation.³¹ Ma et al.³² found that the formation of a few NiAl_2O_4 will favor high activity of Ni/ Al_2O_3 catalyst during methanation, and having an optimum ratio of the easy-reducing NiO_x to the difficult-reducing nickel species may be one of the reasons for the good activity of the studied catalyst. Comparison of methanation performances over Ni-Mg/ Al_2O_3 catalysts prepared with the methods of co-precipitation, homogeneous precipitation and acid-base pairing have clarified that the dispersed NiO interacting with support would prevent the agglomeration of Ni crystallites, and this was likely to improve the activity and stability of the catalyst at high temperatures (up to 973 K).³³

Nonetheless, it is not fully understood how the catalyst activity and stability are influenced by the different nickel species and their interactions with support. The present paper devises the studies of such issues through varying the calcination and

reduction temperatures by clarifying their influences on the properties and methanation performances (activity and stability) of the Ni/Al₂O₃ catalyst.

2. Experimental

2.1. Preparation of Ni-Mg-Zr-La/Al₂O₃ catalysts

The Ni-Mg-Zr-La/Al₂O₃ catalyst with 19 wt% NiO, 8 wt% MgO, 3 wt% ZrO₂ and 5 wt% La₂O₃ was prepared with a method integrating the acid-base pairing and hydrothermal treatment. Here, MgO, La₂O₃ and ZrO₂ were added into the Ni/Al₂O₃ catalyst for these promoters could interact favorably with nickel to inhibit carbon deposition on the catalyst and thus benefit the catalyst for long-term stability.³⁴⁻³⁷ In fact, most commercial methanation catalysts also contain these additives so that the study on Ni-Mg-Zr-La/Al₂O₃ catalyst has also the higher practical value.

In preparing the catalyst, aqueous solutions of NaAlO₂ and metal nitrates including Ni(NO₃)₂·6H₂O, Mg(NO₃)₂·6H₂O, ZrOCl₂·8H₂O, La(NO₃)₃·6H₂O and Al(NO₃)₃·9H₂O were first added dropwise into a reaction vessel with 200 mL water in advance kept at 313 K and under continuous mechanical stirring. The addition rate of the solutions and the ratio of Al(NO₃)₃·9H₂O to NaAlO₂ were controlled to maintain the condition of pH = 11. Then the solution of the precursor was transferred to a stainless steel autoclave which was in turn sealed and maintained at 473 K for 10 h and cooled in turn to room temperature naturally in air. The resulting precipitate was, in succession, aged, washed, filtered, dried at 353 K for 10 h and finally calcined at one of four particularly selected different temperatures (773 K, 873 K, 973 K and 1073 K) for 4 h. The obtained catalysts were all crushed and sieved into particles of

180-230 μm and denoted as CC-773, CC-873, CC-973 and CC-1073 according to their calcination temperatures, respectively.

2.2. Methanation test

The measurement of catalytic activity and stability was conducted via atmospheric methanation tests in a downflow quartz reactor (16 mm i.d.) equipped with a thermocouple at the bottom of the catalyst bed. Prior to the reaction, about 1.5 g of catalyst was reduced by temperature programmed from 393 K to 1073 K in a N_2 -base gas containing 10 vol% H_2 . Then, the temperature of the catalyst bed was decreased to the designated reaction-starting temperature. A gas mixture of $\text{H}_2:\text{CO} = 3:1$ in moles was fed into the reactor to start the methanation reactions. The effluent gas from the reactor was cooled in an ice-water condenser and then dewatered in a column of silica gel before sent to a micro GC (Agilent 3000) for analyzing its molar composition on-line.

The CO conversion and CH_4 concentration referred to herein are defined as

$$X_{\text{CO}} (\%) = \frac{f_{\text{CO},\text{in}} - f_{\text{CO},\text{out}}}{f_{\text{CO},\text{in}}} \times 100$$

and

$$C_{\text{CH}_4} (\%) = \frac{f_{\text{CH}_4,\text{out}}}{f_{\text{CO},\text{out}} + f_{\text{H}_2,\text{out}} + f_{\text{CO}_2,\text{out}} + f_{\text{CH}_4,\text{out}} + f_{\text{N}_2,\text{out}}} \times 100$$

where X is the conversion of CO, C is the CH_4 concentration and f is the volumetric flow rate of the gas species (CO , H_2 , CO_2 , CH_4 or N_2) that was calculated from the GC-analyzed composition and the total gas flow rate determined by taking the well metered flux of N_2 as the internal standard.

2.3. Catalyst Characterization

The surface area and pore size of the catalysts were estimated from the N₂ physisorption curve measured at 77 K via Autosorb-1 (Quantachrome). Prior to measurement, each catalyst sample was thoroughly degassed at 573 K in advance. The crystal structures of the fresh and spent catalysts were analyzed using X-ray power diffractometry (XRD, X'Pert MPD Pro, Panalytical) with Cu K_α radiation of $\lambda = 1.5418 \text{ \AA}$. The temperature-programmed reduction (TPR) and oxidation (TPO) were both carried out using an automated chemisorption analyzer (chem-BET pulsar TPR/TPD, Quantachrome). During TPR, an Ar-base gas containing 10 vol% H₂ was used as the reacting agent and its flow rate was maintained at 120 mL·min⁻¹. A catalyst sample of 50 mg was heated from 393 K to 1273 K at a rate of 5 K·min⁻¹, and the consumed H₂ in the process was monitored with a Mass Spectrometry (MS, Proline, AMETCH). For TPO, 50 mg of the spent catalyst was first pretreated in a He stream at 373 K for 30 min. After cooling naturally, the oxidation test was performed by heating the sample from 373 K to 923 K at a rate of 5 K·min⁻¹ in a N₂-base gas flow containing 10 vol% O₂ and in turn held the sample at 923 K for 60 min to fully oxidize the carbon species on the catalyst. The emitted CO₂ in the TPO test was monitored on-line with the MS. The transmission electron microscopic measurements (TEM) were carried out in the JEOL electron microscope (JEM-2100) with an accelerating voltage of 200 kV.

3. Results and discussion

3.1. Catalyst characterization before methanation

The physisorption results of the catalysts calcined at different temperatures are summarized in Table 1. With increasing the calcination temperature, the BET surface area and pore volume of the catalyst decreased, while the average pore size of the catalyst increased. The surface area decreased significantly from 118 to 52 m²·g⁻¹ as the calcination temperature increased from 773 to 1073 K. These results imply that higher calcination temperature results in the sintering of support and the collapse of small pores, which cause the retention of large pores in the catalyst.

The XRD patterns of the Ni-Mg-Zr-La/Al₂O₃ catalysts calcined at different temperatures are shown in Fig. 1 (a). The NiAl₂O₄, MgAl₂O₄, Ni-Mg solid solution and γ -Al₂O₃ generally co-presented at 2θ around 37°, 45° and 67° in the calcined samples, while the peaks of NiO appeared at 43° and 63° corresponding to the (200) and (220) planes, respectively. With increasing the calcination temperature, the overlapped diffraction peaks of solid solutions and γ -Al₂O₃ slightly shifted to the low diffraction angle. This is because the finely dispersed nickel oxide species in the calcined catalysts were obviously incorporated into the lattice of MgO or γ -Al₂O₃ during the calcination process, resulting in the formation of solid solutions phase.^{38,39} Meanwhile, the formation of nickel aluminate phases retarded the phase transformation in the catalyst due to the increase in activation energy for crystallization of both alumina and nickel oxide species.⁴⁰ Therefore, no phase transformation of alumina (γ -Al₂O₃ to α -Al₂O₃) occurred by increasing the calcination temperature to 1073 K. Subtracting the diffraction peaks of ZrO₂ and La₂O₃, the peak of NiO at $2\theta=43^\circ$ shows the highest intensity for CC-773, while in CC-1073 the

highest intensity was at 2θ of 37° and 45° corresponding to solid solutions. This indicates that the higher calcination temperature, the higher crystallinity of solid solutions showed.

The H_2 -TPR measurements were carried out to clarify the interaction between nickel species and support. Fig. 2 shows the TPR profiles of Ni-Mg-Zr-La/ Al_2O_3 catalysts calcined at different temperatures. The catalysts calcined at 773, 873 and 973 K all exhibited only one reduction band corresponding to the reduction of dispersed nickel oxide that would surely interact with the alumina support. With increasing the calcination temperature, the reduction peak shifted to the higher temperature indicated the increasing difficulty for reducing the nickel oxide. As the calcination temperature increased to 1073 K, two reduction peaks were obviously identified. The peak at low temperature referred to the reduction of the dispersed nickel oxide interacting with the support, while that at high temperature was the reduction of solid solutions phase, i.e., $NiAl_2O_4$ or Ni-Mg solid solution.⁴¹⁻⁴⁹

After reducing by temperature programmed from 393 K to 1073 K at $5\text{ K}\cdot\text{min}^{-1}$ in 10 vol% H_2 of N_2 -base, the four catalysts all showed additional diffraction peaks of metallic Ni at 2θ of 44.5° , 51.8° and 76.3° corresponding to its (111), (200) and (220) planes in Fig. 1 (b), respectively. However, the intensity of the Ni peaks followed an order of CC-1073 < CC-973 < CC-873 < CC-773, which just corresponds to the above-identified fact that the catalyst had less highly dispersed NiO or the NiO is more difficult to be reduced as calcined at higher temperature.

3.2 Methanation performance evaluation

Atmospheric syngas methanation over the prepared Ni-Mg-Zr-La/Al₂O₃ catalysts was tested continuously but alternatively at temperatures of 823 K and 923 K under $SV = 60 \text{ NL}\cdot\text{g}^{-1}\cdot\text{h}^{-1}$. Fig. 3 shows the resulting CO conversion (a) and CH₄ concentration (b) in the product gas for the catalysts calcined at four different temperatures. Before tests, reduction of the catalysts was performed according to the experimental method. In the first 3 h of reaction at 823 K, the tested catalysts followed an activity order of CC-1073 > CC-973 > CC-873 > CC-773 judged by the realized CO conversion in Fig. 3 (a). When increasing the reaction temperature to 923 K which makes the thermodynamic limitation on reactions (methanation and water gas shift reaction) into effect, the CO conversion over all the catalysts obviously decreased, for example, those over the CC-1073 and CC-973 catalysts decreased from 72.5% and 67.7% to 42.1% and 43.3%, respectively. When decreasing again the reaction temperature to 823 K, the CO conversion was almost restored for all the catalysts except for CC-1073, although with very slight decreases in the conversion. Over the CC-1073 catalyst, the CO conversion was back to 65.6%, obviously lower than its original value of 72% for the first test at 823 K. Consequently, the activity order became CC-973 > CC-1073 > CC-873 > CC-773 after the first temperature alternation, and it remained in all the successive alternations between 823 K and 923 K. The results indicate that though the calculation at 1073 K led to the higher initial activity, it has the poorer stability for high-temperature methanation, i.e., at 923 K.

The variations of CH₄ concentration in the product gas shown in Fig. 3 (b) demonstrated the same results. The concentration was 18-22 vol% for the first sets of

tests at 823 K and followed the same order of CC-1073 > CC-973 > CC-873 > CC-773 from high to low CH₄ contents. Alternating the reaction temperature from 823 K to 923 K obviously decreased the CH₄ content in the produced gas to 8-10 vol%, showing the hydrodynamic limitation due to equilibrium as well. Lowering the temperature again to 823 K from 923 K did not fully restore the CH₄ content for CC-1073, and it was only about 18.5 vol% against 21 vol% for the tests at the first 823 K. As for all the other catalysts, the CH₄ content only slightly decreased (less than 1 vol%). These made the order of CH₄ content to become CC-1073 > CC-973 > CC-873 > CC-773, the same as the CO conversion in Fig. 3 (a). For the following temperature alternations between 823 K and 923 K, such an order of relationship in the CH₄ content did not change, while the CH₄ content very slightly decreased with extending the reaction time for all catalysts to indicate their slow deterioration (not fully deactivation) with processing of methanation reactions.

In summary, one can see from Fig. 3 that the catalysts calcined at 773, 873 and 973 K did not have dramatic change in activity and selectivity during alternations of the methanation temperature between 823 K and 923 K. The catalyst calcined at 973 K showed the highest activity and selectivity for methanation, while that at 773 K did the lowest. Consequently, the suitable calcination temperature for the tested Ni-Mg-Zr-La/Al₂O₃ catalyst is possibly about 973 K.

3.3 Characterization of spent catalyst

Fig. 1 (c) shows the XRD patterns of the spent catalysts after the 20-h atmospheric methanation tests that were shown in Fig. 3. Apart from all the species

identified for the reduced catalysts in Fig. 1 (b), graphite can be observed in Fig. 1 (c) at $2\theta = 26.3^\circ$ for the spent catalysts which caused by the carbon deposition. The amount of the deposited carbon for all the catalysts which was measured via an infrared carbon-sulfur analyzer is listed in Table 1. It shows that the deposited carbon amount was the highest for CC-1073 and it followed an order of $CC-1073 > (CC-773 \approx CC-873 \approx CC-973)$. Exactly, the amount for CC-1073 was six times higher than that for the other three catalysts. Comparing with the XRD patterns in Fig. 1 (b), the full width half maximum (FWHM) of the Ni peak at $2\theta = 44.5^\circ$ decreased for spent catalysts, implying an increase in the crystal size of metallic nickel. The increasing degree of this crystal face followed an order of $CC-1073 (0.1338^\circ) > CC-773 (0.0502^\circ) > CC-973 (0.0256^\circ) \approx CC-873 (0.0233^\circ)$.

Referring to the previous study,³³ at least two types of deposited carbon would be found on the Ni/Al₂O₃ catalysts. The first assigned to the reactive amorphous carbon (C_α) was oxidized around 550 K or below 680 K, while the oxidation of the second type was at temperatures above 680 K (e.g., 680-930 K) to indicate its nature as the inactive graphitic carbon (C_γ). Fig. 4 shows the TPO curves of all the spent catalysts. It can be seen that the oxidation of the carbon on CC-1073 occurred in a wide temperature range of 530-900 K, while for the other catalysts this occurred between 740 K and 900 K. This indicates that both C_α and C_γ were deposited on the surface of the CC-1073 catalyst, whereas for the other catalysts it was mainly C_γ. Meanwhile, the CC-1073 had a distinctively large peak of released CO₂ than all the other three catalysts did. This complies with its highest intensity of diffraction peak for graphite

shown in Fig. 1 (c) and also the highest carbon amount measured in Table 1 for CC-1073. It has been reported that for high-temperature methanation (e.g., >800 K), the formed reactive carbon (C_α) would convert to inactive graphitic (C_γ) to encapsulate the metal particles and plug micro and meso pores to speed up the deactivation of catalyst.⁵⁰ Therefore, for high-temperature methanation (>800 K), the catalyst deactivation would be mainly due to the formed inactive carbon (C_γ). The much higher inactive carbon deposition as well as the large amount of active carbon C_α for CC-1073 clarified that it is much easier to form carbon deposition over this catalyst and thus causes catalyst deactivation, as was demonstrated by the methanation tests shown in Fig. 3.

Fig. 5 shows the TEM images of the Ni-Mg-Zr-La/Al₂O₃ catalysts calcined at different temperatures. For the reduced catalysts in the first row one can see that the Ni particles (black spots) were uniformly dispersed and the average size based on 50 Ni particles was found to be about 12 nm, 19 nm and 10 nm for the reduced CC-773, CC-973 and CC-1073, respectively. After methanation for about 20 hours in Fig. 3, metal sintering was identified for the CC-773 and CC-1073 samples in Fig. 5 (d) and (f). For the spent CC-1073 in Fig. 5 (f), the average Ni particle size was estimated to be about 42 nm, and carbon nanofibers obviously presented on the surface of the catalyst, as shown with the dashed-line circle. The carbon deposition requires some adjacent nickel atoms, and the catalyst with the larger nickel particles is more vulnerable to deposit carbon than that with the smaller particles.^{51, 52} Although CC-773 and CC-1073 had the similar nickel particle sizes, the latter had obviously

lower surface area to cause its more adjacent nickel atoms to make it easily occur the carbon deposition for higher carbon deposition.

The possibly weak interaction between nickel oxide and support increased the amount of Ni^0 exposing on the surface of the reduced CC-773 catalyst. This in turn accelerated the loss and sintering of the active Ni, as verified in Fig. 5 (a) and 5 (d) where the average Ni particle size increased by about 39 nm by the 20-h continuous methanation test. If the interaction between nickel oxide and the support is strong enough, an active site Ni^0 formed in catalyst reduction would be surrounded by several Al_2O_3 molecules.⁵³ This thus hinders the aggregation of Ni^0 and improves the catalyst stability. As justified in Fig. 5 (e), there was only a slight change in the Ni particle size for the catalyst calcined at 973 K (CC-973) after the 20-h methanation reaction. The average Ni particle size was found to be 25 nm for the spent CC-973, which would be the proper crystal size (about 20-100 nm) for methanation.^{5,54}

The catalyst calcined at high temperature as 1073 K possessed a small surface area (Table 1) but strong interaction between nickel oxide and support (Fig. 2) leading to small dispersed metallic nickel particles (Fig. 5 (c)). The realized CO conversion was initially the highest for this catalyst in spite of its least active sites. The surface area was actually too small to disperse the active sites so that the growth and sintering rate of Ni particles was higher. Thus, its larger Ni particles accelerated the carbon deposition. The more deposited carbon and also fewer active surfaces would both deactivate the CC-1073 catalyst. As a consequence, a moderate metal-support interaction in the Ni/ Al_2O_3 catalyst would be necessarily needed for high activity and

high stability of a catalyst for syngas methanation.

3.4 Further justification by deep reduction

In order to further study the role of metal-support interaction (or NiAl_2O_4), the sample of CC-973 was reduced in a N_2 -base gas containing 10 vol% H_2 via a temperature program from 393 K to 973 K or 1073 K and further maintained at such temperatures for 1 h. The obtained catalysts were denoted as CR-973 and CR-1073, respectively. Fig. 6 (a) compares the XRD patterns of the calcined CC-973 and its further reduced samples of CR-973 and CR-1073. The reduction caused obvious diffraction peaks of metallic nickel at 44.7° , 51.9° and 76.5° to represent the (111), (200) and (220) planes, respectively. With raising the reduction temperature (from 973 K to 1073 K), the intensities of such nickel peaks all became more obvious to show higher peak intensities for CR-1073. This result implies there are more Ni^0 with larger crystal size in the catalyst reduced at 1073 K than that in CR-973. Meanwhile, it also shows the increased reduction degree at higher reduction temperature.

Fig. 7 (a) shows the H_2 -TPR diagrams for the preceding catalysts. For the original CC-973 (calcined) catalyst, only one reduction peak was observed above 850 K and at a peak temperature of 997 K. The reduced samples had essentially two peaks, one centering at a temperature below 700 K and the other between 1150 K and 1180 K. The results obviously show that the lower temperature of H_2 consumption in Fig. 7 (a) should be attributed to the reduction of NiO formed as the reduced catalyst was exposed to air and partially oxidized. Correspondingly, the higher temperature of H_2 consumption should be assigned to the reduction of nickel aluminates. In order to

further verify the two types of nickel species, the H₂-TPR analysis was also conducted for CR-973 and CR-1073 after they experienced a TPO test which is being heated from 373 K to 923 K at a rate of 5 K·min⁻¹ in a N₂-base gas flow containing 10 vol% O₂ and in turn held at 923 K for 60 min. From Fig. 7 (b) one can also identify two reduction peaks for both the catalysts. One was at 690-730 K and the other at 1090-1180 K. The former should represent the actually available active sites in the catalyst for syngas methanation that is usually at temperatures below 973 K. Via the base line in Fig. 7 (b) one can calculate the ratio S1/S2 of the two reduction peaks in H₂-TPR. It shows essentially the amount ratio of the reduced NiO to nickel aluminates, thus quantifying the reduction degree of nickel species. The reduction extent is then higher for CR-1073 than for CR-973 because the values of S1/S2 were 17.4 and 1.6, respectively. In fact, at 1073 K most of nickel aluminate was reduced, as shown by the H₂-TPR curve of the original CC-973 sample in Fig. 7 (a).

Fig. 8 shows the variations of CO conversion and CH₄ concentration in the product gas for atmospheric methanation performances over the catalysts CR-973 and CR-1073 in alternating the reaction temperature between 823 K and 923 K. The adopted conditions were a H₂ flow of 240 mL·min⁻¹, a CO flow of 80 mL·min⁻¹ and a *SV* of 27 NL·g⁻¹·h⁻¹. Overall, the performance was much better over CR-973 than over CR-1073. Although raising the reaction temperature from 823 K to 923 K decreased the CO conversion from 71% to 38% over CR-973, this lowered conversion was still 30% higher than the highest CO conversion realized over CR-1073. In the continuous 25-h test, the CO conversion and also CH₄ content in the product gas slightly

decreased with reaction time over both the catalysts. This shows that there was slight deactivation of the catalysts. Correlating with Fig. 7 (a) shows that the CR-973 had relatively less active NiO sites but obvious nickel aluminates, which made it possess the higher activity in Fig. 8. The too high reduction degree at 1073 K, which removed most nickel aluminates, resulted in obviously lower activity and also lower stability of the catalyst for methanation.

Fig. 6 (b) shows the XRD patterns of the spent catalysts after the methanation tests in Fig. 8. An obvious diffraction peak at $2\theta = 26.3^\circ$ revealed the deposition of graphite on the surface of CR-1073 during the atmospheric methanation. The total carbon amount from the infrared carbon-sulfur analysis shows that the CR-1073 catalyst had a distinctively high carbon deposition of 31.9 wt%, whereas the deposited carbon on CR-973 was only 5.0 wt% for the same tested time in Fig. 8. The distinctively different amounts of deposited carbon for both CR-973 and CR-1073 were further demonstrated in the TPO tests shown in Fig. 9. There, the CO₂-emission peak appeared around 830 K indicated the inactive graphite carbon C_γ, while the emission peak was distinctively larger for CR-1073 than for CR-973.

Fig. 10 shows the TEM images of the different catalysts based on CC-973. The NiO particles were uniformly dispersed in Fig. 10 (a) with an average particle size of 7 nm for the original CC-973 (calcination only). After reduction, the average Ni crystal size was about 15 nm in Fig. 10 (b) for CR-973 and 24 nm in Fig. 10 (d) for CR-1073. Thus, the too high reduction temperature converted most nickel and caused the most serious sintering of Ni⁰ to lower the methanation activity and its stability. Fig.

10 (c) shows that the methanation via Fig. 8 did not significantly affect the morphology of the catalyst CR-973 (versus 10 (b)). For the spent CR-1073 in Fig. 10 (e), though its average Ni crystal size was about 25 nm (against Fig. 10 (d)), some aggregated large Ni particles were obviously present on the catalyst. This would not only decrease the number of active sites and the active surface but also accelerate the carbon deposition on the catalyst to quickly deactivate the catalyst.

As a consequence, one can conclude from the above tests that certain nickel aluminate in the catalyst is indispensable to the expected activity and also stability of the Ni/Al₂O₃ catalysts for syngas methanation at high temperatures such as above 823 K. Ruckenstein et al.⁵⁵ found that the strong metal-support interaction weakens the catalytic activity of nickel but it also hinders the Boudouard reaction which is the major source of carbon deposition in methanation. The nickel crystallites decorated with discontinuous interfacial layer of nickel aluminate is also considered to be critical for high sintering resistance of the Ni/Al₂O₃ catalyst.⁵⁶ Overall, it can be seen that it is critically important to optimize the ratio of two types of nickel species in the methanation catalyst for ensuring the good catalytic activity and stability.

4. Conclusions

The necessary metal-support interaction in Ni-Mg-Zr-La/Al₂O₃ catalyst for syngas methanation at high temperatures was studied through varying the calcination and reduction temperatures during catalyst preparation. It was found that the calcination temperature significantly affects the structural and chemical properties of the catalysts. Raising the calcination temperature increased the interaction between

nickel and support but lowered the surface area of the catalyst. Atmospheric syngas methanation over the prepared catalysts was tested continuously but alternatively at 823 K and 923 K. After reduced by temperature programmed to 1073 K, the catalyst calcined at 1073 K exhibited the highest initial activity at 823 K in spite of its least active sites. However, the surface area was too small to disperse the active sites, thus causing a higher sintering rate of Ni particles and more hard-oxidizing carbon was also formed in methanation at high temperatures.

The similar methanation tests over the catalyst calcined at 973 K but reduced at different temperatures revealed that the sample with the lower ratio of reduced NiO to nickel aluminates (1.6) from the reduction at 973 K showed the higher activity, better stability and less carbon deposition than that reduced at 1073 K with the higher ratio (17.4) that implies the deep reduction of all Ni species. All of these results show consequently that only the Ni/Al₂O₃ catalyst with moderate interaction between metal and support leading to the coexistence of NiO and nickel aluminates at suitable ratios, such as the catalyst calcined and reduced at 973 K, can have reasonably good and stable activity for syngas methanation at temperatures above 823 K. Nonetheless, more studies are required to clarify the optimal ratios between such two types of nickel species.

Acknowledgement

The authors are grateful to the financial support of National Natural Science Foundation of China (21161140329), International Science & Technology Cooperation Program of China (2013DFG60060) and National Key Technology R&D

Program (2012BAC03B05).

References

- 1 S. Therdtthianwong, C. Siangchin and A. Therdtthianwong, *Fuel Process. Technol.*, 2008, **89**, 160-168.
- 2 M. Zangouei, A. Z. Moghaddam and M. Arasteh, *Chem Eng. Res. Bull.*, 2010, **14**, 97-102.
- 3 S. Hwang, J. Lee, U. G. Hong, J. G. Seo, J. C. Jung, D. J. Koh, H. Lim, C. Byun and I. K. Song, *J. Ind. Eng. Chem.*, 2011, **17**, 154-157.
- 4 J. Gao, C. Jia, M. Zhang, F. Gu, G. Xu and F. Su, *Catal. Sci. Technol.*, 2013, **3**, 2009-2015.
- 5 S. Takenaka, T. Shimizu and K. Otsuka, *Int. J. Hydrogen Energy*, 2004, **29**, 1065-1073.
- 6 L. C. Loc, N. Tuan, N. K. Dung, N. Phuc and H. S. Thoang, *Advanced, Nature, Science*, 2006, **7**, 91-105.
- 7 J. Hu, C. Yu, Y. Bi, L. Wei, J. Chen and X. Chen, *Chin. J. Catal.*, 2014, **35**, 8-20.
- 8 C. Yu, J. Hu, K. Yang, X. Liu and Q. Fan, *Chin. J. Rare Metal.*, 2014, **38**, 60-69.
- 9 Y. W. Chung, G. Xiong and C. C. Kao, *J. Catal.*, 1984, **85**, 237-243.
- 10 F. Mariño, G. Baronetti, M. a. Jobbagy and M. Laborde, *Appl. Catal., A*, 2003, **238**, 41-54.
- 11 D. Liu, X. Y. Quek, W. N. E. Cheo, R. Lau, A. Borgna and Y. Yang, *J. Catal.*, 2009, **266**, 380-390.
- 12 C. Yu, J. Hu, W. Zhou and Q. Fan, *J. Energy Chem.*, 2014, **23**, 235-243.
- 13 C. Mirodatos, H. Praliaud and M. Primet, *J. Catal.*, 1987, **107**, 275-287.
- 14 Y. Yu, G. Q. Jin, Y. Y. Wang and X. Y. Guo, *Fuel Process. Technol.*, 2011, **92**, 2293-2298.
- 15 M. Agnelli, M. Kolb and C. Mirodatos, *J. Catal.*, 1994, **148**, 9-21.
- 16 J. Rostrup-Nielsen, K. Pedersen and J. Sehested, *Appl. Catal., A*, 2007, **330**, 134-138.
- 17 J. Sehested, J. A. Gelten, I. N. Remediakis, H. Benggaard and J. K. Nørskov, *J.*

- Catal.*, 2004, **223**, 432-443.
- 18 A. Djaidja, S. Libs, A. Kiennemann and A. Barama, *Catal. Today*, 2006, **113**, 194-200.
- 19 Z. Xu, Y. Li, J. Zhang, L. Chang, R. Zhou and Z. Duan, *Appl. Catal., A*, 2001, **213**, 65-71.
- 20 L. Avdeeva, O. Goncharova, D. Kochubey, V. Zaikovskii, L. Plyasova, B. Novgorodov and S. K. Shaikhutdinov, *Appl. Catal., A*, 1996, **141**, 117-129.
- 21 R. Yang and J. Chen, *J. Catal.*, 1989, **115**, 52-64.
- 22 R. Yang, C. Xing, C. Lv, L. Shi and N. Tsubaki, *Appl. Catal., A*, 2010, **385**, 92-100.
- 23 F. Frusteri, L. Spadaro, F. Arena and A. Chuvilin, *Carbon*, 2002, **40**, 1063-1070.
- 24 J. D. Bellido, J. E. De Souza, J. C. M'Peko and E. M. Assaf, *Appl. Catal., A*, 2009, **358**, 215-223.
- 25 H. S. Roh, K. W. Jun, S. C. Baek and S. E. Park, *Catal. Lett.*, 2002, **81**, 147-151.
- 26 P. Panagiotopoulou, D. I. Kondarides and X. E. Verykios, *J. Phys. Chem. C*, 2011, **115**, 1220-1230.
- 27 Y. Wang, R. Wu and Y. Zhao, *Catal. Today*, 2010, **158**, 470-474.
- 28 J. N. Park and E. W. McFarland, *J. Catal.*, 2009, **266**, 92-97.
- 29 A. Zhao, W. Ying, H. Zhang, H. Ma and D. Fang, *Catal. Commun.*, 2012, **17**, 34-38.
- 30 K. Urasaki, Y. Tanpo, T. Takahiro, J. Christopher, R. Kikuchi, T. Kojima and S. Satokawa, *Chem. Lett.*, 2010, **39**, 972-973.
- 31 P. Kim, Y. Kim, H. Kim, I. K. Song and J. Yi, *Appl. Catal., A*, 2004, **272**, 157-166.
- 32 M. Shengli, T. Yisheng and H. Yizhuo, *J Nat. Gas Chem.*, 2011, **20**, 6.
- 33 J. Liu, J. Yu, F. Su and G. Xu, *Catal. Sci. Technol.*, 2014, **4**, 472.
- 34 S. Wang and G. Lu, *Appl. Catal., B*, 1998, **16**, 269-277.
- 35 K. Tomishige, O. Yamazaki, Y. Chen, K. Yokoyama, X. Li and K. Fujimoto, *Catal. Today*, 1998, **45**, 35-39.
- 36 J. M. Wei, B. Q. Xu, J. L. Li, Z. X. Cheng and Q. M. Zhu, *Appl. Catal., A*, 2000,

- 196**, L167-L172.
- 37 K. Y. Koo, H.-S. Roh, Y. T. Seo, D. J. Seo, W. L. Yoon and S. B. Park, *Appl. Catal., A*, 2008, **340**, 183-190.
- 38 J. R. Ross, M. C. Steel and A. Zeini-Isfahani, *J. Catal.*, 1978, **52**, 280-290.
- 39 J. G. Seo, M. H. Youn, D. R. Park, J. C. Jung and I. K. Song, *Catal. Lett.*, 2009, **132**, 395-401.
- 40 T. Klimova, M. L. Rojas, P. Castillo, R. Cuevas and J. Ramírez, *Microporous Mesoporous Mater.*, 1998, **20**, 293-306.
- 41 K. Y. Koo, H.-S. Roh, Y. T. Seo, D. J. Seo, W. L. Yoon and S. Bin Park, *Int. J. Hydrogen Energy*, 2008, **33**, 2036-2043.
- 42 K. Y. Koo, H.-S. Roh, U. H. Jung, D. J. Seo, Y.-S. Seo and W. L. Yoon, *Catal. Today*, 2009, **146**, 166-171.
- 43 X. Zhang, J. Liu, Y. Jing and Y. Xie, *Appl. Catal., A*, 2003, **240**, 143-150.
- 44 L. Qu, W. Zhang, P. J. Kooyman and R. Prins, *J. Catal.*, 2003, **215**, 7-13.
- 45 T. Borowiecki, W. Gac and A. Denis, *Appl. Catal., A*, 2004, **270**, 27-36.
- 46 H. Lu, H. Yin, Y. Liu, T. Jiang and L. Yu, *Catal. Commun.*, 2008, **10**, 313-316.
- 47 R. Yang, X. Li, J. Wu, X. Zhang, Z. Zhang, Y. Cheng and J. Guo, *Appl. Catal., A*, 2009, **368**, 105-112.
- 48 A. Romero, M. Jobbágy, M. Laborde, G. Baronetti and N. Amadeo, *Catal. Today*, 2010, **149**, 407-412.
- 49 H. Li, Y. Xu, C. Gao and Y. Zhao, *Catal. Today*, 2010, **158**, 475-480.
- 50 C. H. Bartholomew, *Appl. Catal., A*, 2001, **212**, 17-60.
- 51 Y. Bang, J. G. Seo and I. K. Song, *Int. J. Hydrogen Energy*, 2011, **36**, 8307-8315.
- 52 D. Trimm, *Stud. Surf. Sci. Catal.*, 1988, **36**, 39-50.
- 53 J. Zieliński, *J. Catal.*, 1982, **76**, 157-163.
- 54 J. J. Gao, C. M. Jia, J. Li, F. N. Gu, G. W. Xu, Z. Y. Zhong and F. B. Su, *Ind. Eng. Chem. Res.*, 2012, **51**, 10345-10353.
- 55 E. Ruckenstein and Y. H. Hu, *Appl. Catal., A*, 1995, **133**, 149-161.
- 56 P. Bolt, F. Habraken and J. Geus, *J. Catal.*, 1995, **151**, 300-306.

Table 1 Physical properties from N₂ physisorption isotherms and carbon amount on spent catalysts for Ni-Mg-Zr-La/Al₂O₃ calcined at different temperatures.

| Catalyst | Surface area ^a | Pore volume ^b | Average pore size ^c | Carbon amount ^d |
|----------|---------------------------|--------------------------|--------------------------------|----------------------------|
| CC-773 | 118 | 0.32 | 8.3 | 4.3 |
| CC-873 | 93 | 0.25 | 9.2 | 4.2 |
| CC-973 | 79 | 0.22 | 9.8 | 3.9 |
| CC-1073 | 52 | 0.18 | 12.7 | 25.3 |

^a Calculated with the BET equation from the N₂ physisorption isotherms, m²·g⁻¹.

^b Referring to the BJH desorption pore volume from the N₂ physisorption isotherms, cm³·g⁻¹.

^c Referring to the BJH desorption average pore size from the N₂ physisorption isotherms, nm.

^d Measured via an infrared carbon-sulfur analyzer (CS-344, US) for spent catalysts, wt%.

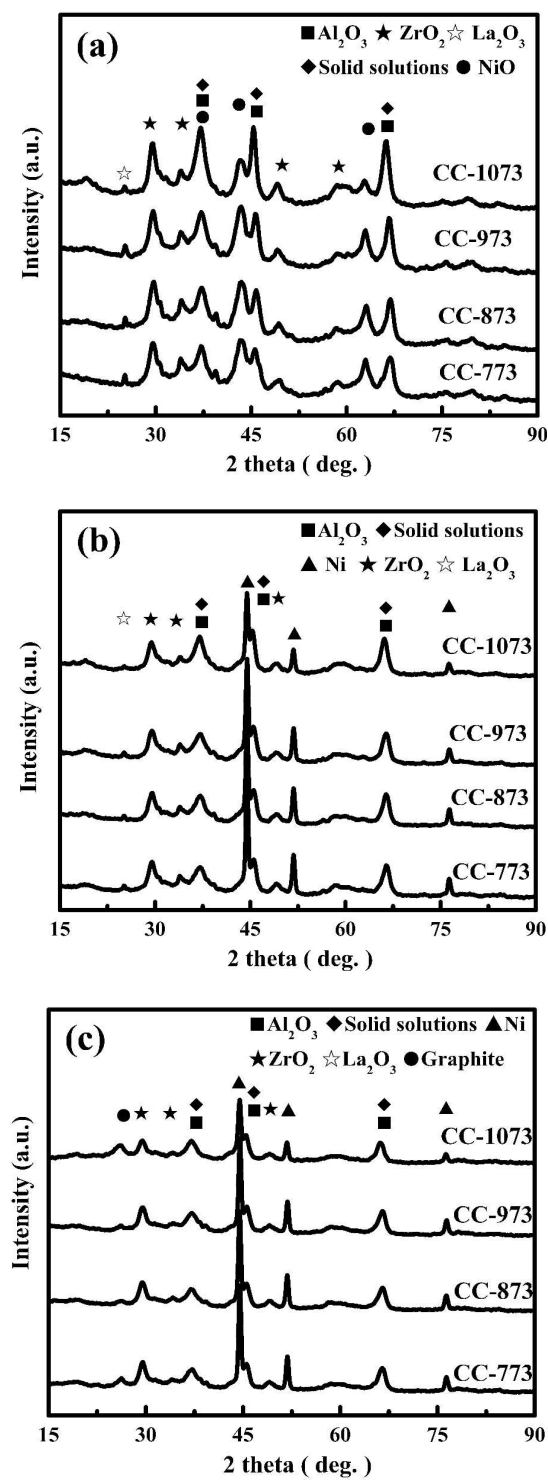


Fig. 1 XRD patterns of (a) calcined, (b) reduced and (c) spent Ni-Mg-Zr-La/Al₂O₃ catalysts calcined at different temperatures in preparation (solid solutions include NiAl₂O₄, MgAl₂O₄ and Ni-Mg solid solution).

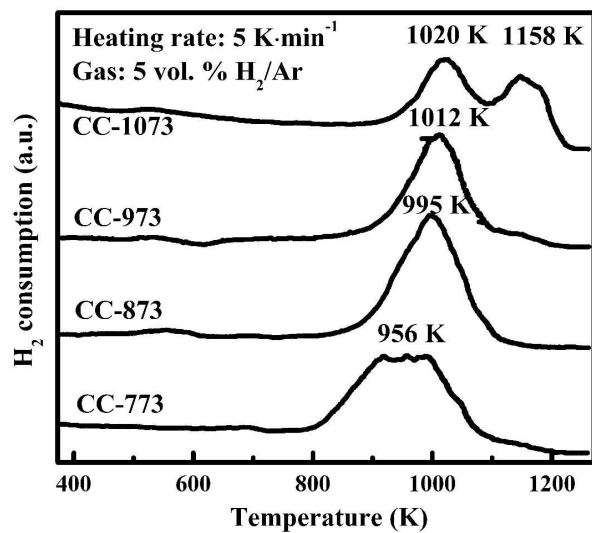


Fig. 2 H₂-TPR profiles of Ni-Mg-Zr-La/Al₂O₃ catalysts calcined at different temperatures in preparation.

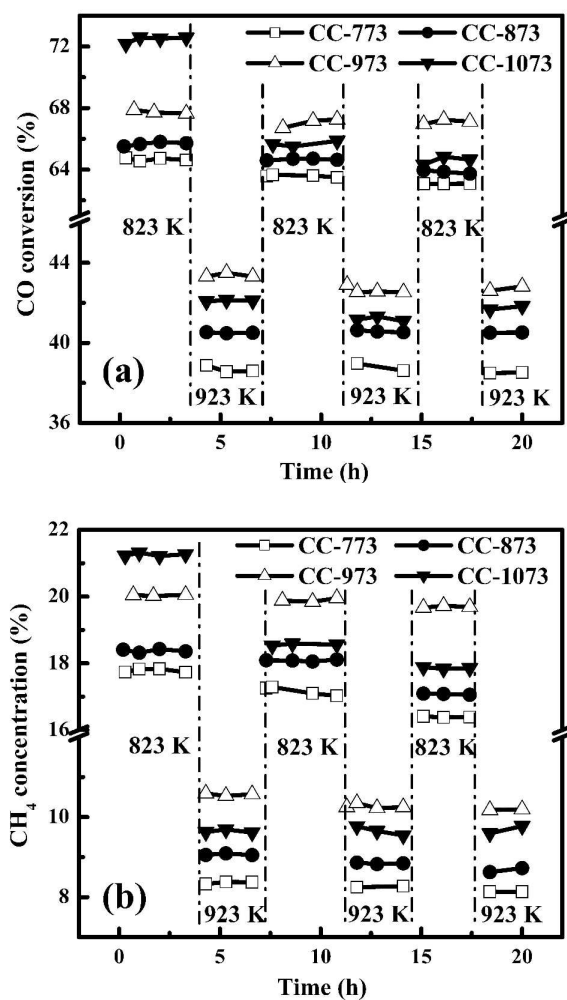


Fig. 3 Variations of (a) CO conversion and (b) CH₄ concentration in effluent gas with reaction time in alternating reaction temperature between 823 K and 923 K for atmospheric methanation over reduced Ni-Mg-Zr-La/Al₂O₃ catalyst calcined at different temperatures in preparation ($SV = 60 \text{ NL} \cdot \text{g}^{-1} \cdot \text{h}^{-1}$).

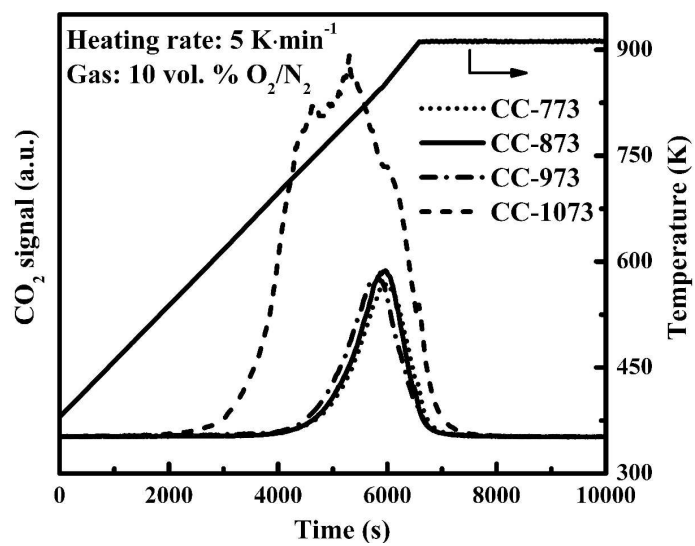


Fig. 4 TPO profiles of spent Ni-Mg-Zr-La/Al₂O₃ catalysts after 20-h methanation shown in Fig. 3.

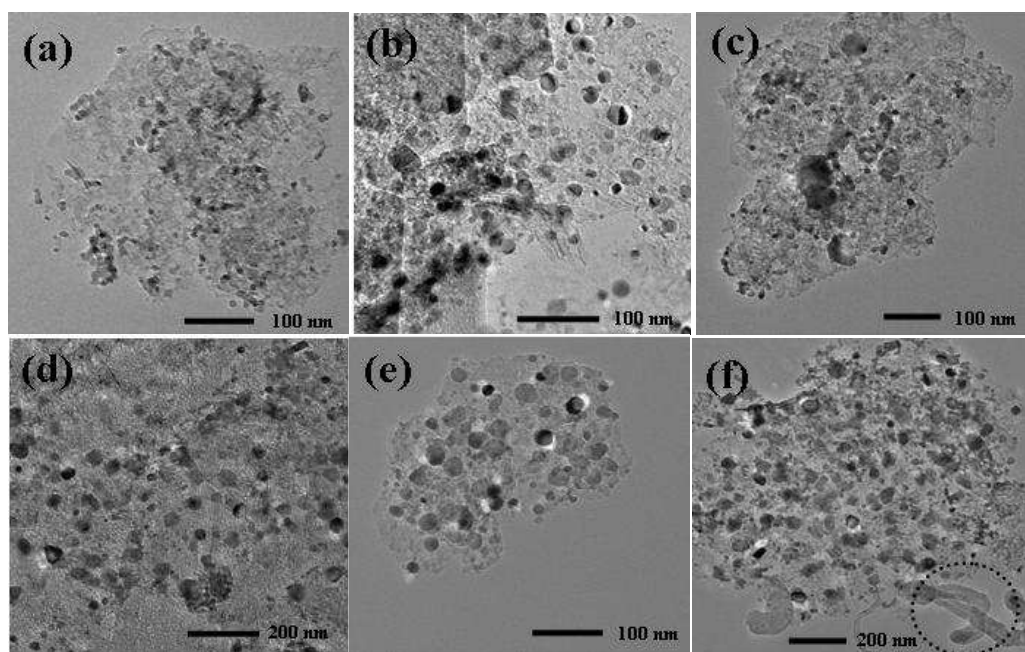


Fig. 5 TEM images of reduced and spent Ni-Mg-Zr-La/Al₂O₃ catalysts for (a) reduced CC-773, (b) reduced CC-973, (c) reduced CC-1073, (d) spent CC-773, (e) spent CC-973 and (f) spent CC-1073.

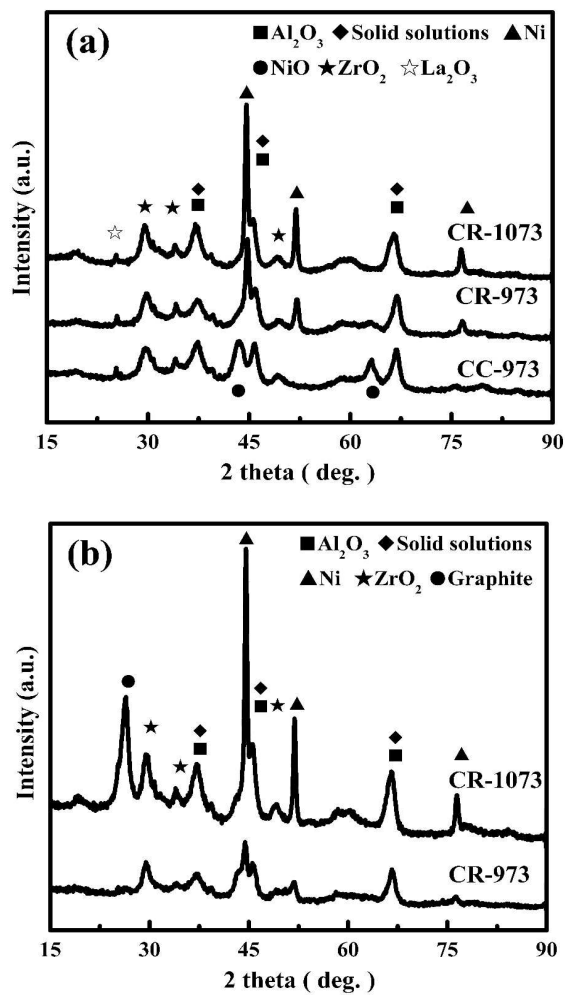


Fig. 6 XRD patterns of CC-973 catalyst (a) reduced at different temperatures and (b) after methanation over such catalysts (solid solutions include NiAl₂O₄, MgAl₂O₄ and Ni-Mg solid solution).

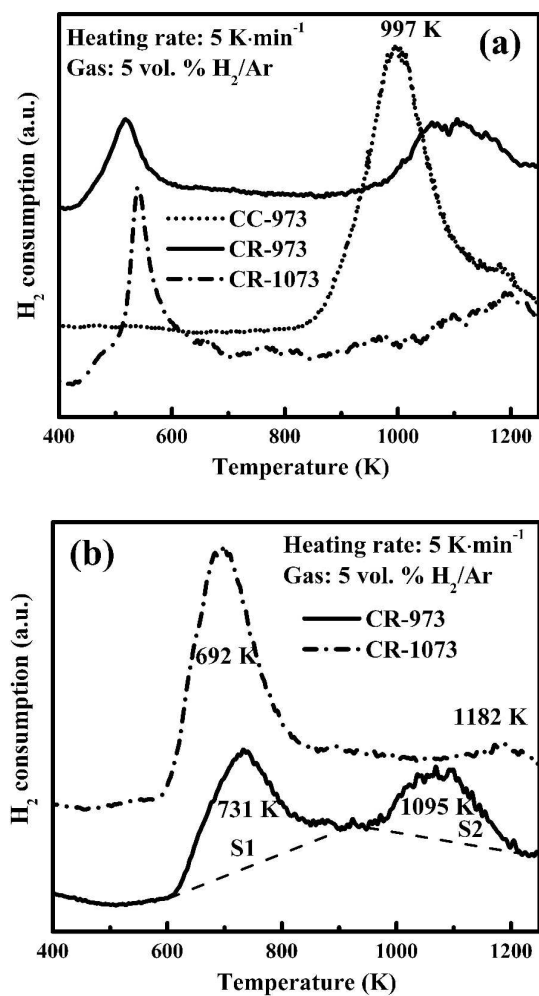


Fig. 7 H_2 -TPR profiles of CC-973 catalyst (a) reduced at different temperatures and (b) after TPO test that is being heated from 373 K to 923 K at a rate of 5 $\text{K}\cdot\text{min}^{-1}$ in a N_2 -base gas flow containing 10 vol% O_2 and in turn held at 923 K for 60 min. .

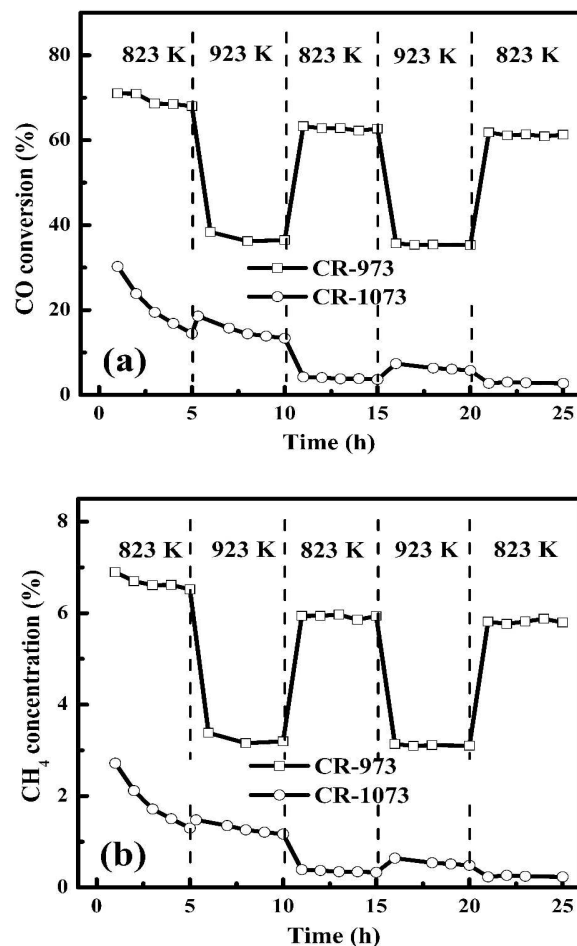


Fig. 8 Variations of (a) CO conversion and (b) CH₄ concentration in effluent gas with reaction time in alternating reaction temperature between 823 K and 923 K for atmospheric methanation over CC-973 reduced at 973 K and 1073 K ($SV = 27 \text{ NL} \cdot \text{g}^{-1} \cdot \text{h}^{-1}$).

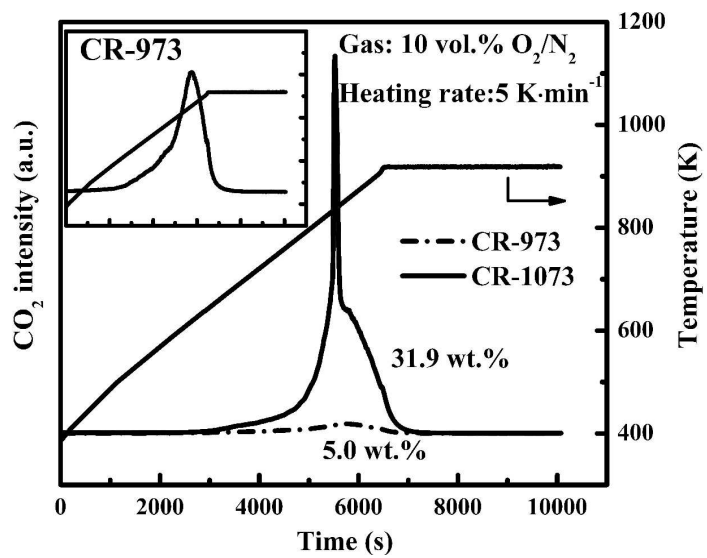


Fig. 9 TPO results of spent CR-973 and CR-1073 after atmospheric methanation tests for 25 h as shown in Fig. 8.

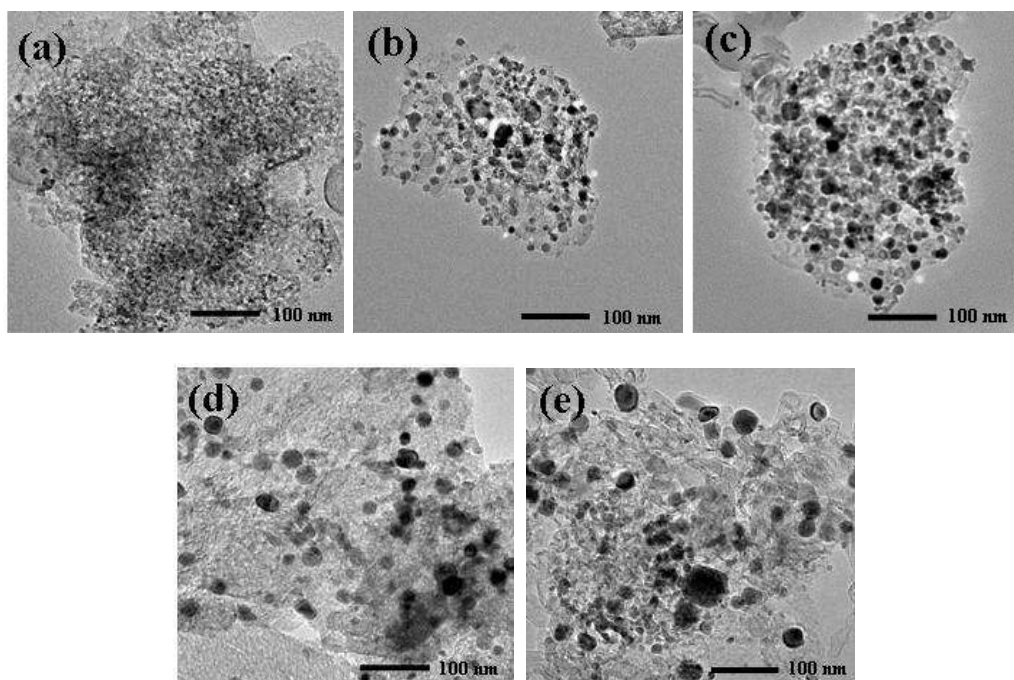


Fig. 10 TEM images of catalysts (a) CC-773 (calcined only), (b) CR-973, (c) spent CR-973, (d) CR-1073 and (e) spent CR-1073.

Atmospheric syngas methanation tests conducted continuously but at 823 K and 923 K alternatively over Ni-Mg-Zr-La/Al₂O₃ catalysts made with different calcination and reduction temperatures has demonstrated that only the catalyst with moderate metal-support interaction, such as that calcined and further reduced at 973 K so that it has both free NiO species and nickel aluminates, can have reasonably good and stable activity for syngas methanation at high temperatures such as above 823 K.

